Available online at www.sciencedirect.com
ScienceDirect
Catalysis Today 133–135 (2008) 200–209
CATALYSIS TODAY
www.elsevier.com/locate/cattod

Carbon dioxide reforming of methane over La_2NiO_4 as catalyst precursor—Characterization of carbon deposition

Germán Sierra Gallego [a,b], Fanor Mondragón [b], Jean-Michel Tatibouët [a], Joël Barrault [a], Catherine Batiot-Dupeyrat [a,*]

[a] *Laboratoire de Catalyse en Chimie Organique, UMR CNRS 6503, Université de Poitiers, Ecole Supérieure d'Ingénieurs de Poitiers, 40 Avenue du Recteur Pineau, 86022 Poitiers Cedex, France*
[b] *Institute of Chemistry, University of Antioquia, A.A. 1226, Medellín, Colombia*

Available online 1 February 2008

Abstract

La_2NiO_4-type perovskites were prepared by the ''self-combustion'' method and were used as catalyst precursor for the CO_2 reforming of CH_4 reaction at 700 °C. The catalysts were used in reduced and non-reduced form. High CH_4 and CO_2 conversions were obtained with a H_2/CO ratio lower than 1. This result was explained by the occurrence of the RWGS (reverse water gas shift) reaction. The reduction of the perovskite La_2NiO_4 leads to the formation of small nickel particles (average diameter: 7 nm), consequently the catalytic activity is higher than that obtained with 5% Ni/La_2O_3 (average diameter: 11 nm).

The use of the perovskite La_2NiO_4 without reductive treatment prior to the reaction shows that the catalyst is composed of a mixture of Ni, $La_2O_2CO_3$ and La_2NiO_4 during the first hours of the reaction. The catalytic activity is thus lower than that obtained with the reduced perovskite. The reaction performed using the non-reduced perovskite is accompanied by carbon deposition. TEM and Raman analysis showed that multiwalled carbon nanotubes are formed under those experimental conditions.

Keywords: CO_2 reforming of CH_4; Perovskite La_2NiO_4; Auto combustion method

1. Introduction

In recent years, the carbon dioxide reforming of methane process has received considerable attention from both academic and industrial sectors. This reaction converts the cheapest carbon containing gases (CH_4 and CO_2) in synthesis gas with a H_2/CO ratio of 1. This process is particularly interesting environmentally when gas fields contain a significant amount of methane and carbon dioxide, both gases being undesirable greenhouse gases. The low H_2/CO ratio is preferentially used for the production of liquid hydrocarbons in the Fischer–Tropsch synthesis and for the production of formaldehyde and polycarbonates [1,2].

Because of the high endothermicity of the reaction, the process can be used in energy transfer from solar energy to chemical energy, in energy storage in the form of CO and H_2 and chemical energy transmission systems (CETS) [3].

The main drawbacks of the process are: (1) requirement of temperatures as high as 800 °C for high conversions and (2) catalyst deactivation due to carbon deposition. The two main reasons for coke formation are: methane decomposition (reaction (7)) and the Boudouard reaction (reaction (6)). The first reaction is favored at high temperatures and low pressures, whereas the second one is favored at low temperatures and high pressures.

The carbon dioxide reforming of methane is accompanied by some side reactions [4]:

$$CH_4 + CO_2 \Leftrightarrow 2CO + 2H_2 \quad (\text{carbon dioxide reforming}) \tag{1}$$

$$H_2 + CO_2 \Leftrightarrow CO + H_2O \quad (\text{reverse water gas shift}) \tag{2}$$

$$CO_2 + 4H_2 \Leftrightarrow CH_4 + 2H_2O \quad (CO_2\ \text{methanation}) \tag{3}$$

$$CO + 3H_2 \Leftrightarrow CH_4 + H_2O \quad (\text{CO methanation}) \tag{4}$$

$$CH_4 + 2H_2O \Leftrightarrow CO + 3H_2 \quad (\text{steam reforming}) \tag{5}$$

* Corresponding author. Tel.: +33 549453540.
E-mail address: catherine.batiot.dupeyrat@univ-poitiers.fr (C. Batiot-Dupeyrat).

0920-5861/$ – see front matter
doi:10.1016/j.cattod.2007.12.075

$$2CO \Leftrightarrow C + CO_2 \quad \text{(Boudouard reaction)} \tag{6}$$

$$CH_4 \Leftrightarrow C + 2H_2 \quad \text{(methane decomposition)} \tag{7}$$

$$C + H_2O \Leftrightarrow CO + H_2 \quad \text{(coke gasification)} \tag{8}$$

Several authors reported carbon deposition and catalytic deactivation during CO_2 reforming of CH_4 over different catalysts [5,6].

Thermodynamic calculation of graphitic carbon deposition as related to reaction conditions suggested that carbon formation could be avoided thermodynamically at high temperatures (e.g., ±1000 °C) and also by the presence of excess of CO_2, H_2O or O_2 [7–11]. However, from a standpoint of industry, it is desirable to operate the process at a relatively lower temperature and with a CO_2/CH_4 ratio close to unity. Another alternative is to find catalysts resistant to coke formation.

Considerable research efforts have been directed to the development of catalysts which show high activity towards synthesis gas formation and are also resistant to coking. Numerous supported metal catalysts have been used for this reaction. Among them supported noble metal (Rh, Ru, Ir, Pt, and Pd) [12–22] and nickel [23–27] show high catalytic performance in terms of methane conversion and selectivity to synthesis gas. Catalysts based on noble metal are less sensitive to carbon deposits than those based on nickel. However, considering the high cost and limited availability of noble metals, it is more advantageous to develop nickel-based catalysts with good resistance to carbon deposition and a high activity during extended period of time. In previous papers we have shown that $LaNiO_3$ perovskite used as catalyst precursor leads to a very active catalyst for the CO_2 reforming of CH_4 [28,29].

Currently, there are three technologies for synthesis gas production: MIDREX [30], CALCOR [7,31] and SPARG [32,33,26,34,35]. The last two processes were developed for CO_2 reforming of CH_4. The principle of SPARG (sulfur passivated reforming) allows carbon free operation by adding sulfur to the process stream, which block the sites for carbon formation while sufficient sites for reforming reactions are maintained. The CALCOR process uses an excess of CO_2 to inhibit carbon deposition. Nevertheless, only recently the first pilot plant for synthesis gas production was successfully operated in Japan [36]. In this process, natural gas is fed to the reactor with CO_2 and H_2O to obtain a synthesis gas with a ratio H_2/CO equal to 2.

The aim of the present work was to investigate the activity and stability of the K_2NiF_4-type precursor: La_2NiO_4. We particularly focused on the reaction mechanism involved using the catalyst with or without reductive treatment prior to the reaction.

The catalytic performances were compared with those of Ni/$La_2O_2CO_3$ and Ni/La_2O_3. The conventional Ni/La_2O_3 was used as a reference catalyst as suggested by Verykios and co-worker [37].

2. Experimental

2.1. Catalysts preparation

The K_2NiF_4-type oxide La_2NiO_4 was prepared by the self-combustion method [38]. Glycine ($H_2NCH_2CO_2H$) used as ignition promoter was added to an aqueous solution of metal nitrates with appropriate stoichiometry, in order to obtain a ratio $NO_3^-/NH_2 = 1$. The resulting solution was slowly evaporated until a vitreous green gel was obtained. The gel was heated up to around 250 °C, temperature at which the ignition reaction occurs producing a powdered precursor which still contains carbon residues. Calcination at 700 °C for 6 h eliminates all of the remaining carbon and leads to the formation of the K_2NiF_4 structure.

Ni/La_2O_3 catalysts containing 1%, 5% and 17% were prepared by the wet impregnation method using nitrate salt as metal precursor. Nickel nitrate was dissolved in distilled water. Then the appropriated amount of La_2O_3 was added under continuous stirring. The slurry was heated up to 90 °C and kept at this temperature until the water was evaporated. The residue was then dried at 110 °C for 24 h and subsequently calcined at 700 °C under air for 6 h until complete decomposition of nitrates was obtained. After this treatment, the catalysts were reduced at 700 °C in pure H_2 for 1 h.

5% Ni/$La_2O_2CO_3$ was prepared using the impregnation method described above. The $La_2O_2CO_3$ material was prepared by CO_2 treatment of commercial La_2O_3 during 2 h at 700 °C.

2.2. Characterization

The catalysts were characterized by powder X-ray diffraction using a Siemens D-5000 diffractometer with Cu $K\alpha_1$ = 1.5406 Å and Cu $K\alpha_2$ = 1.5439 Å, operated at 40 kV and 30 mA. The diffraction patterns were recorded in the 2θ value range of 10–90° with a step size of 0.01° and 1 s per step. The XRD in situ experiments were conducted in a Bruker D5005 equipment using Cu $K\alpha_1$ radiation. The diffractometer was equipped with an Anton Paar KG reactor chamber mounted on a goniometer. The powdered samples were placed on a filament of kenthel (FeCrAl) with cavity and pressed by hand. For in situ X-ray diffraction, a mixture of 3% H_2 in He was used with a flow rate of 50 mL/min, the temperature was raised from ambient to 973 K. Prior to the diffraction measurements the samples were purged under helium for 30 min at room temperature.

TEM was carried out on a Philips CM120 instrument, with LaB_6 filament and equipped with an energy dispersive X-ray analyzer (EDX). TEM images of deposited carbon were taken after treatment of the sample with a solution of 65% HNO_3. The sample was deposited on a Cu grid for TEM observation.

Raman spectra of carbon nanotubes were performed by diluting the sample in KBr, using a Perkin Elmer Spectum GX–IR FT Raman spectroscopy with a diode Nd:YAG laser and a wavelength of 514.5 nm from 10 to 4000 cm^{-1}.

TPR and H_2 chemisorption experiments were carried out in a Micromeritics Autochem 2910 using about 160 mg of catalyst.

TPR experiments were performed using 5% H_2/Ar flow while the temperature rise at 5 °C/min from ambient to 700 °C and maintained at this temperature for 2 h. Then the system was purged in Ar at 720 °C for 6 h and cooled to 50 °C. Hydrogen-pulsed chemisorption was started at 50 °C using 5% H_2/Ar and repeated at 5 min intervals until the hydrogen area peaks became identical. The amount of hydrogen consumed was measured with a thermal conductivity detector. Metal dispersion on the surface was calculated assuming the adsorption stoichiometry of one hydrogen atom per nickel surface atom ($H/Ni_s = 1$).

XPS characterization was performed using an Axis Ultra Kratos spectrometer equipped with Al Kα X-ray radiation source in a vacuum of 2×10^{-9} Torr. La 3d, Ni 3p,O 1s and C 1s signals were measured.

The surface areas were measured by BET procedure using nitrogen–helium adsorption. All samples were degassed with He for 30 min at 623 K before measurement, the adsorption–desorption isotherm of N_2 was determined using 30% N_2/He as the adsorbate on a Micromeritics Flowsorb II 2300 apparatus at −196 °C.

2.3. Catalytic reaction

The catalysts were tested in a fixed bed continuous flow quartz reactor (i.d. = 6 mm) at atmospheric pressure. The flow rate of the reactant mixture was 100 mL/min (CH_4/CO_2/He = 10/10/80 mL/min; GHSV = 3.0×10^5 mL g^{-1} h^{-1}) over a 20 mg catalyst bed. The temperature was increased from room temperature to 700 °C at a rate of 5 °C/min, and maintained at this temperature for the desired reaction time. The temperature was measured with a thermocouple located inside the reactor but without direct contact with the catalyst.

In some experiments the perovskite catalyst precursor was used without pre-treatment and in some cases after reduction under hydrogen at 700 °C for 1 h. The reaction products were analyzed by an on-line mass spectrometer. The detection limit was estimated to be around 0.04 μmol. According to the intensity of the signal measured by the MS, this value corresponds to about 1% of the total amount detected.

3. Results and discussion

3.1. Temperature-programmed reduction and in situ XRD

In order to obtain information about the behavior of La_2NiO_4 under reductive atmosphere (H_2), TPR experiments followed by in situ XRD analyses were performed.

The in situ X-ray diffraction is shown in Fig. 1 and the TPR profile of La_2NiO_4 is shown in Fig. 2.

The XRD pattern of the perovskite La_2NiO_4 after calcination at 700 °C (Fig. 1a) reveals the presence of a very crystalline tetragonal La_2NiO_4 (K_2NiF_4-type structure).

The in situ X ray diffraction analysis shows that until 500 °C (Fig. 1f), the structure of La_2NiO_4 is preserved; it begins to change at around 600 °C (Fig. 1g); at this temperature a mixture of La_2NiO_4 and La_2O_3 is clearly identified. At 700 °C, La_2NiO_4 was completely destroyed, the only phases detected being Ni and La_2O_3 (Fig. 1h).

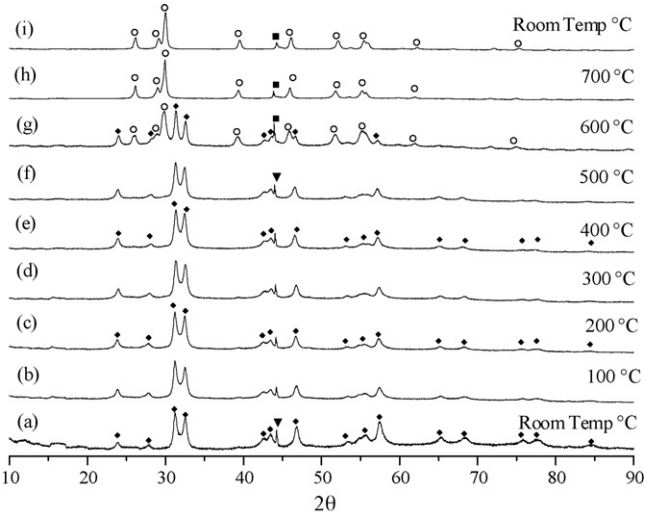

Fig. 1. In situ XRD patterns of La_2NiO_4 during the reduction treatment. (■) Ni; (○) La_2O_3; (◆) La_2NiO_4; (▼) sample holder signal.

The TPR profile of La_2NiO_4 shows two main peaks (Fig. 2). The first one is small with a maximum at around 380 °C and the second one which starts evolving at around 500 °C.

The first peak of TPR between 300 and 420 °C does not correspond to a modification of the perovskite structure according to the in situ XRD experiments, but it could be assigned to the reduction of the excess of oxygen in $La_2NiO_{4+\delta}$. It has been shown in the literature that the non-stoichiometry level can reach $\delta = 0.18$ [39].

The second peak appears between 530 and 680 °C and corresponds to a complete reduction of the perovskite according to:

$$La_2NiO_4 + H_2 \rightarrow Ni + La_2O_3 + H_2O$$

TPR and in situ XRD experiments confirm that a complete reduction of La_2NiO_4 in Ni and La_2O_3, requires a temperature

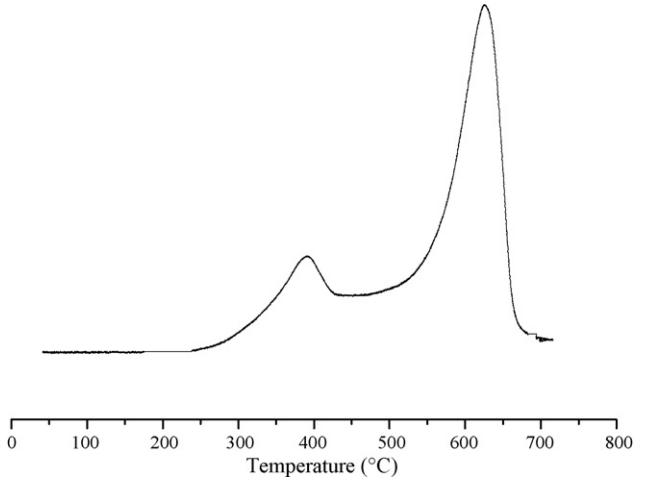

Fig. 2. TPR curves of the perovskites La_2NiO_4. Catalyst weight: 160 mg; gas flow rate: 5% H_2/Ar, 50 mL/min.

higher than 680 °C under H_2 and the reduction occurs in one step. Contrary to $LaNiO_3$ which requires 580 °C and three steps for its total reduction [28].

3.2. X-ray diffraction characterization

The XRD patterns of La_2NiO_4 after reduction and after reaction are shown in Fig. 3. After reduction treatment, the K_2NiF_4 structure does not exist, but Ni and La_2O_3 are detected (Fig. 3c). After 15 h of reaction the only phases detected are the hexagonal lanthanum oxo-carbonate $La_2O_2CO_3$ and Ni with both starting catalysts reduced and non-reduced (Fig. 3e). The XRD analysis performed after 1 h at 700 °C under reactant mixture using the non-reduced material, shows that La_2NiO_4 is not completely reduced but a mixture of Ni, $La_2O_2CO_3$ and non-reduced La_2NiO_4 is present (Fig. 3d). This result is in accordance with the TPR profiles showing that La_2NiO_4 can be completely reduced at a temperature as high as 700 °C under pure H_2.

3.3. Characterization by electron microscopy

Using TEM micrographs it was possible to determine the particle size distribution of the reduced and non-reduced catalysts after 15 h of reaction (Figs. 4 and 5). The histograms data are normalized to 100 particles while about 500 particles were measured.

The formation of small Ni particles is obtained by reduction under hydrogen of La_2NiO_4. The size distribution is narrow: 2–30 nm, with an average diameter of 7 nm after the reduction step and 10 nm after 15 h of reaction. After reaction, large particles of nickel (up to 140 nm) are observed using the catalyst without reductive treatment prior to the reaction, whereas the use of the reduced catalyst leads to the presence of nickel particles smaller than 22 nm (Fig. 4).

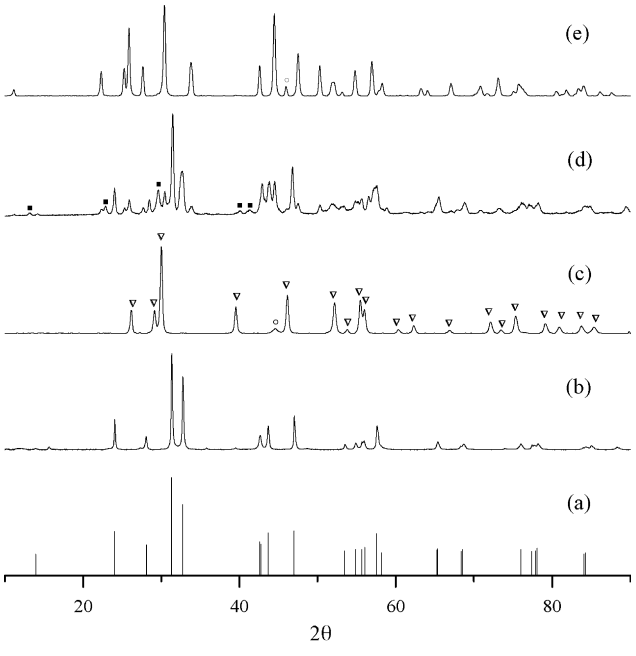

Fig. 3. XRD patterns of the La_2NiO_4 precursor material: (a) PDF 89-3460, (b) prepared catalyst before reaction: La_2NiO_4, (c) after reduction under hydrogen at 700 °C, (d) after 1 h of reaction at 700 °C over the non-reduced material, and (e) after 15 h of reaction using the non-reduced or reduced material. (°) Ni; (▽) La_2O_3; (◇) $La_2O_2CO_3$ hexagonal; (■) $La_2O_2CO_3$ monoclinic.

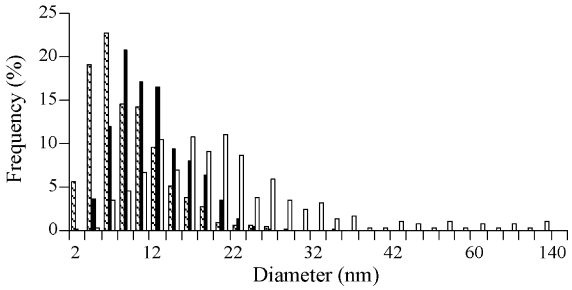

Fig. 4. Particle size distribution determined from TEM measurements for La_2NiO_4. Hatched: catalyst reduced under hydrogen; black: after reaction using reduced catalyst; white: after reaction using non-reduced catalyst.

Thus, we can assume that the nature of the support is very important for the nickel dispersion. The presence of non-reduced La_2NiO_4 during reaction seems to be responsible for the existence of large Ni particles. The nickel particles would sinter at the surface of La_2NiO_4 due to high mobility. When the perovskite is used after reductive treatment, $La_2O_2CO_3$ is easily formed, during the heating step, by CO_2 adsorption, the presence of these carbonate species would stabilize the nickel particles hindering their sintering. In order to confirm the role of the oxycarbonate species towards the nickel dispersion a catalyst was prepared by impregnating nickel over $La_2O_2CO_3$ support.

Fig. 5 shows the nickel dispersion obtained for 5% Ni–$La_2O_2CO_3$ and 5% Ni–La_2O_3.

It appears that the particle size distribution is narrower for 5% Ni–$La_2O_2CO_3$ compared to 5% Ni–La_2O_3. The average nickel particle size of the different species is shown in Table 1.

The results support the finding that the oxycarbonate species allow to obtain a better nickel dispersion at the surface of the support, the average nickel particles being equal to 8 nm at the surface of $La_2O_2CO_3$ against 11 nm at the surface of La_2O_3.

For the Ni/La_2O_3 catalyst, the increase of the diameter of the Ni particles with the nickel loading was observed. Thus, for 17% Ni/La_2O_3 the range of Ni particles is between 2 and 130 nm, with an average of 19 nm accompanied by the formation of nickel agglomerates. These large Ni particles could be responsible for the carbon deposition observed with 17% Ni/La_2O_3.

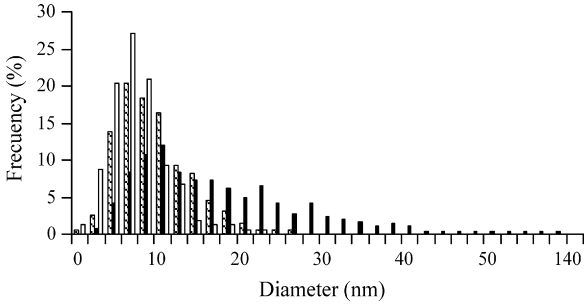

Fig. 5. Particle size distribution determined from TEM measurements. Hatched: 5% Ni/La_2O_3; black: 17% Ni/La_2O_3; white: 5% Ni/$La_2O_2CO_3$.

Table 1
Average nickel particle size derived from TEM and XRD for La_2NiO_4, 1, 5, 17% La_2O_3 and 5% $La_2O_2CO_3$

	Catalyst	Average nickel particle size (nm)
La_2NiO_4	After reduction	7
	After reaction over reduced catalyst	10
	After reaction over unreduced catalyst	20
1% Ni/La_2O_3	Reduced	11
5% Ni/La_2O_3	Reduced	Average: 11
17% Ni/La_2O_3	Reduced	Agglomerates + Ni average: 19
5% $Ni/La_2O_2CO_3$	Reduced	Average: 8

3.4. H_2 chemisorption

The hydrogen chemisorption was used to estimate the amount of accessible metallic nickel particles at the surface of the catalyst. The results gathered in Table 2 show that the hydrogen uptake is very low whatever the catalyst. The small amount of metallic nickel on La_2O_3 has been ascribed to different factors or a combination of them:

(1) The presence of thin layers of La_2O_3 partially cover the metal species as proposed by Bell and co-workers using a Pd/La_2O_3 catalyst [40,41]. Similarly, different authors [42,41] have suggested the blocking of nickel crystallites by LaO_x species with Ni/La_2O_3 catalyst [43].
(2) The strong metal–support interaction could reduce the amount of H_2 adsorbed specially at very low nickel loadings [43].
(3) Another possibility that can cause the same effect is the presence of strongly chemisorbed hydrogen on the metal particles, formed during the reduction step, which inhibits any further hydrogen chemisorption. Nevertheless, at present time, the nature of the interaction between Ni and La_2O_3 or La_2O_x is still unclear. The results here obtained suggest that after the reduction step only a small amount of nickel particles at the surface of the catalyst can be observed by hydrogen chemisorption.

Table 2
H_2 chemisorption (at 50 °C) data for reduced La_2NiO_4, 1, 5, 17% La_2O_3 and 5% $La_2O_2CO_3$ catalysts

Catalyst reduced at 700 °C	H_2 uptake ($\mu mol\ g^{-1}$)	% Ni disponible	Ni loading (wt%)[a]
La_2NiO_4	7.0	0.6	15.5
1% Ni/La_2O_3	[b]	[b]	1.3
5% Ni/La_2O_3	1.8	0.42	5.5
17% Ni/La_2O_3	21.2	0.77	17.3
5% $Ni/La_2O_2CO_3$	[b]	[b]	5.0

[a] CHN analysis.
[b] Negligible.

Table 3
Surface composition of the La_2NiO_4 catalyst after reduction treatment and after reaction from XPS signal

Catalyst	Surface concentration (at.%)					Ni state
	La	O	C	Ni	La/Ni	
After reduction	8.6	45.2	43.5	2.8	3.1	100% Ni
After 15 h of reaction using reduced La_2NiO_4	7.7	37.3	53.4	1.6	4.8	37% oxidized Ni

3.5. XPS analysis

The elemental surface composition of the catalyst after reduction and after 15 h of reaction using the reduced perovskite was investigated by XPS; the results are shown in Table 3. The carbon content may arise from atmospheric contamination during transfer to the XPS instrument. The surface carbonate species can be formed due to the interaction of ambient CO_2 with the sample [44]. In the reduced material, the amount of nickel (2.8%) is lower than the amount of lanthanum (8.6%) suggesting that the nickel dispersion on La_2O_3 is large, which is in agreement with TEM micrographs. Moreover, the La/Ni ratio is higher than expected it could be a consequence of the presence of lanthanum oxide at the surface of the catalyst. The reduction of La_2NiO_4 allows to obtain only metallic nickel even at the surface of the catalyst (as shown by the measurement of the nickel state), whereas during the reaction nickel is partially oxidized (37%) most probably as NiO.

After the reaction the ratio La/Ni is slightly increased, it can be due to the presence of carbonate species at the surface of the catalyst, which may cover the nickel particles [45].

3.6. Catalytic performance of the reduced La_2NiO_4

In order to keep the experiments within the region of intrinsic kinetics the reactions were carried out using catalyst grain sizes of about 180 μm. The amount of catalyst was fixed at 20 mg with a total flow rate of 100 mL/min which corresponds to a space velocity of $3 \times 10^5\ mL\ h^{-1}\ g^{-1}$, in order not to reach the thermodynamic equilibrium. The experiment was run for 160 h, the CH_4 and CO_2 conversions and H_2/CO molar ratio are reported in Fig. 6. High conversions

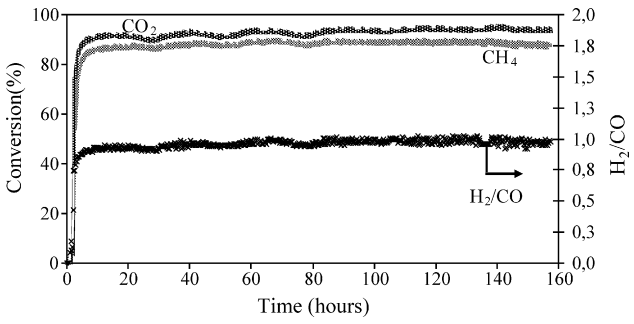

Fig. 6. CH_4 and CO_2 conversion. Molar ratio: H_2/CO; catalyst: 20 mg La_2NiO_4 reduced under hydrogen at 700 °C for 120 h; reaction temperature: 700 °C.

Table 4
CH_4, CO_2 conversions, H_2/CO ratio, BET and carbon deposition determined by elemental analysis (in wt%) after 15 h of reaction

Catalyst precursor	Conversion after 15 h of reaction (%)		Molar ratio, H_2/CO	Carbon deposition (wt%)	BET (m^2/g)
	CH_4	CO_2			
Reduced La_2NiO_4	85	93	0.93	2.7[a]	11
Non-reduced La_2NiO_4	82	88	0.90	70[b]	6
1% Ni/La_2O_3	32	48	0.47	2.6[b]	10
5% Ni/La_2O_3	64	75	0.75	3.2[b]	13
17% Ni/La_2O_3	67	75	0.84	12.0[b]	12
5% Ni/$La_2O_2CO_3$	70	78	0.81	4.3[b]	7

CH_4/CO_2/He: 10/10/80; catalyst weight: 20 mg; flow: 100 mL min^{-1}; T = 700 °C, catalyst reduced under hydrogen at 700 °C prior to the reaction.
[a] After a reaction time of 160 h.
[b] After a reaction time of 15 h.

are reached after 2 h of reaction at 700 °C with values above 85 and 93% for CH_4 and CO_2, respectively, a H_2/CO ratio of 0.93. During the catalytic test the methane and carbon dioxide conversions remain unchanged. Elemental analysis of the catalyst after the above experiment reveals that no carbon deposition was observed after 160 h of reaction (see Table 4).

3.7. Catalytic performance of the non-reduced material

The behavior of La_2NiO_4 as catalyst precursor, without treatment prior to the reaction, is shown in Fig. 7. The conversions of methane and carbon dioxide increase slowly after the temperature has reached 700 °C. The catalytic activity is governed by the slow reduction step of La_2NiO_4 under reactants and products (H_2 and CO). A complete reduction of La_2NiO_4 proceeds between 1 and 15 h of reaction according to XRD analysis. With the current data the exact time of the complete reduction of the catalyst is not possible to be determined. After 15 h of reaction high conversions were obtained (CH_4 = 82% and CO_2 = 88%) while the H_2/CO molar ratio remained slightly lower than 1. For both, reduced and non-reduced material the catalytic activity is almost identical after 15 h of reaction, whereas using La_2NiO_4 without reduction treatment, carbon deposits were found after reaction (see Table 4).

It is accepted that carbon deposition in the dry reforming of methane results from methane decomposition or from the Boudouard reaction as follows:

$$CH_4 \rightarrow C + 2H_2$$

$$2CO \rightarrow C + CO_2$$

Nevertheless, we have shown in a previous paper [46], that the carbon deposition results mainly from the methane decomposition.

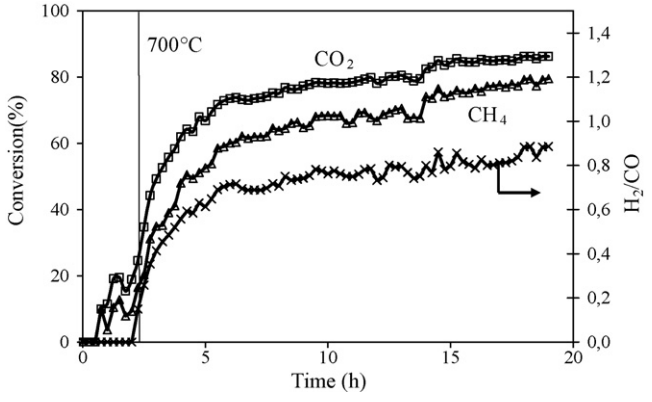

Fig. 7. CH_4 and CO_2 conversion. Molar ratio: H_2/CO; catalyst: 20 mg La_2NiO_4 non-reduced; reaction temperature: 700 °C.

3.8. Comparison of the catalytic activity of La_2NiO_4, Ni/La_2O_3 and Ni/$La_2O_2CO_3$

The performance of La_2NiO_4 as catalyst precursor was compared with that of Ni/La_2O_3 and Ni/$La_2O_2CO_3$ containing various amount of nickel. The conventional Ni/La_2O_3 was used as a reference catalyst as suggested by Verykios and co-worker [37]. The results obtained after 15 h of reaction are displayed in Table 4. BET measurements were performed on the fresh La_2NiO_4 material and after reductive treatment of La_2NiO_4, Ni/La_2O_3 and Ni/$La_2O_2CO_3$.

The surface areas are low whatever the nature of the catalyst is. The reduction of the perovskite phase leads to an increase of the surface area resulting from the structure modification from K_2NiF_4-type to the hexagonal structure of La_2O_3.

Among all the catalyst tested, the reduced perovskite La_2NiO_4 shows the best catalytic activity whereas its surface area is the same as that of Ni/La_2O_3 catalyst. The high activity using perovskite precursors can be explained by the formation of relatively small nickel particles by the reductive treatment, such observation is in accordance with the work of Gao and co-workers [47,48] using La_2NiO_4. The methane conversion is slightly lower than the carbon dioxide conversion. The value of the molar ratio H_2/CO is lower than 1 and the absence of carbon deposits after the reaction indicates that the RWGS (reverse water gas shift) reaction takes place under experimental conditions described here.

$$CO_2 + H_2 \rightarrow CO + H_2O \quad (\text{RWGS})$$

The elemental analysis of the catalyst after the reaction reveals that the amount of carbon is around 3%, which correspond to the amount of carbon in $La_2O_2CO_3$. This result confirms that no

coke deposition is formed after 15 h of reaction except for the 17% Ni/La_2O_3 catalyst (see Table 1).

For Ni/La_2O_3 catalysts, the increase in the nickel loading leads to an increase in the CH_4 and CO_2 conversions. Nevertheless, the reduced La_2NiO_4 material shows higher catalytic performance whatever the amount of deposited nickel was. The well-defined La_2NiO_4 precursor structure may play a crucial role in the high activity as proposed by Guo et al. [49], highly dispersed and stable Ni metal is formed in situ on the catalyst during the reduction step. The better activity of La_2NiO_4 cannot only be attributed to the presence of small nickel particles. The accessibility of nickel particles should also be considered. XPS analysis showed that after reaction the amount of accessible nickel is lower than before reaction. This may be attributed to the partial covering of nickel particles by carbonate species. The low hydrogen uptake with $Ni/La_2O_2CO_3$ corroborates the idea that the presence of carbonate species can limit the accessibility of nickel. With 5% $Ni/La_2O_2CO_3$ the number of active sites (accessible nickel particles) would be too low, which could explain the lower activity of 5% $Ni/La_2O_2CO_3$ compared to La_2NiO_4 precursor, whereas the nickel particles size is very close for both materials.

Comparing the 5% Ni/La_2O_3 with the 5% $Ni/La_2O_2CO_3$ we can observe that the lanthanum oxycarbonate show higher CH_4 and CO_2 conversions than the lanthanum oxide support. This result suggests that the support plays an important role in the reaction by dispersing the active species.

3.9. Influence of contact time

The influence of contact time on conversions of methane and carbon dioxide over La_2NiO_4 catalysts was investigated at 700 °C modifying the gas hourly space velocity (GHSV). The variation in the GHSV was realized by adjusting the amount of catalyst (5, 20 and 50 mg) in a feed consisting of CH_4/CO_2/He = 10/10/80 mL/min, respectively.

As shown in Fig. 8, both the methane and carbon dioxide conversion decreases as GHSV increases. The results obtained using reduced La_2NiO_4 are compared with those reported in the literature. Fig. 8 shows that the La_2NiO_4 perovskite as catalyst precursor exhibit better catalytic activity than 17% Ni/La_2O_3 prepared by the wet impregnation method especially for GHSV values higher than 2.0×10^5 mL g^{-1} h^{-1}. Verykios and co-worker [50] reported CH_4 and CO_2 conversions of 43 and 56%, respectively, using GHSV of 3.0×10^5 mL g^{-1} h^{-1} (contact time = 0.01 g s/mL), whereas in our experiments, for similar GHSV values, we obtained 85 and 93% conversion for methane and carbon dioxide, respectively.

3.10. Suggested reaction mechanism

When the reduced perovskite is used as starting material, CO_2 is adsorbed on La_2O_3 at the reaction conditions to form oxycarbonate species such as $La_2O_2CO_3$. On the other hand, it is known that CH_4 is weakly adsorbed on La_2O_3 [53] while CH_4 is easily activated on metallic Ni particles at high temperatures as shown by theoretical and experimental studies [54,55]. Thus,

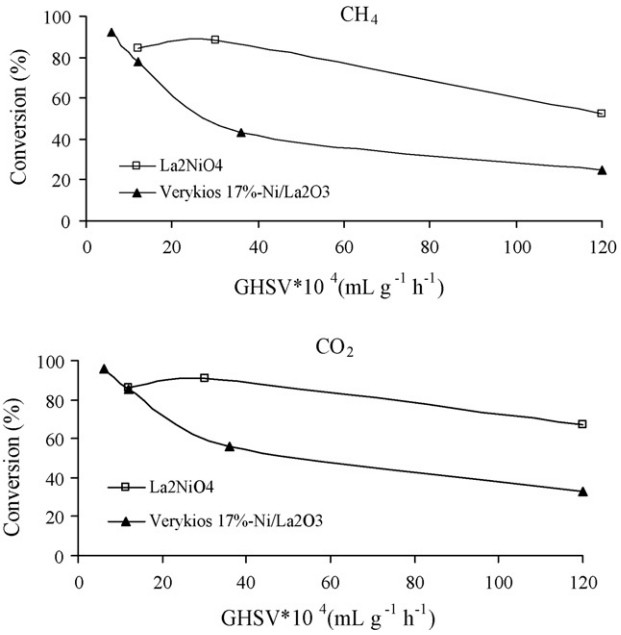

Fig. 8. Influence of contact time on conversion obtained over La_2NiO_4 as precursor of Ni/La_2O_3 compared with 17% Ni/La_2O_3 reported by Verykios and co-worker [53].

it was proposed that under CH_4/CO_2 mixture CH_4 is mainly decomposed on the Ni crystallites to form H_2 and surface carbon species Ni–CH_x, while CO_2 is adsorbed on the La_2O_3 support to form $La_2O_2CO_3$. At high temperatures $La_2O_2CO_3$ may react with the surface carbon species formed on the Ni crystallites to produce CO restoring the Ni surface to its original state. If the rate of carbon deposition is equal to the rate of carbon scavenging no deactivation is observed. We propose a reaction mechanism using the reduced material as schematically depicted in Fig. 9.

This mechanism is in accordance with the reaction paths described in the literature [42,50–52]. The occurrence of the catalytic reaction at the Ni–$La_2O_2CO_3$ interfacial area was proved by Verykios et al. using isotopic tracing techniques [52]. The present results show that the oxygen species from $La_2O_2CO_3$ participate to a significant extent in the formation of CO in the CH_4/CO_2 reaction. Thus the oxycarbonate might be considered as a dynamic pool as shown in Fig. 9.

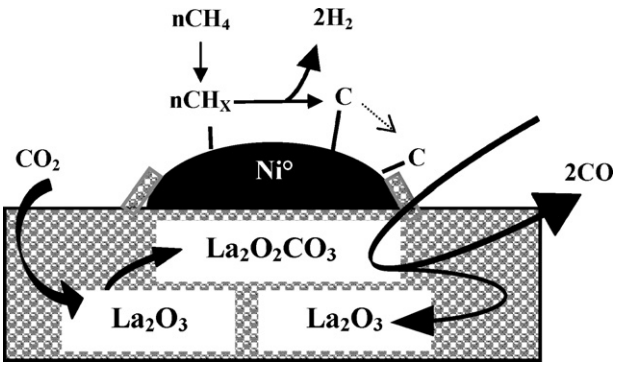

Fig. 9. Proposed mechanism for the role of Ni particles during CO_2 reforming of CH_4 using La_2NiO_4 reduced as precursor of La_2O_3.

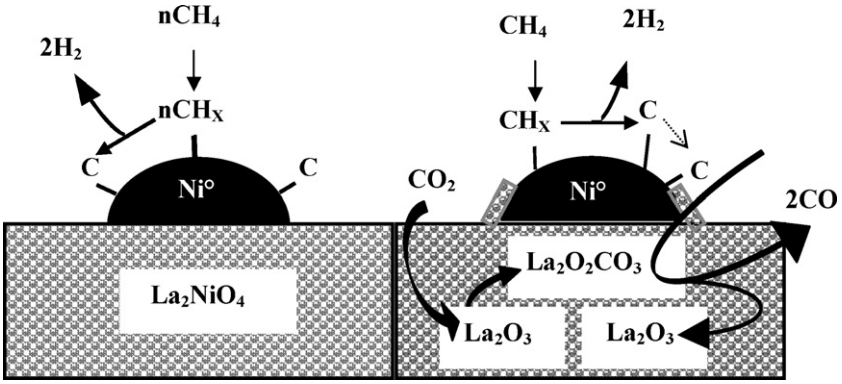

Fig. 10. Proposed mechanism for the CO_2 reforming of CH_4 using La_2NiO_4 non-reduced as precursor of La_2O_3.

Using the non-reduced La_2NiO_4 as starting material, we showed that the perovskite La_2NiO_4 is still present during the first few hours of reaction time. Thus, we can assume that isolated metallic nickel particles can be present at the surface of the support La_2NiO_4. Carbon deposits at the surface of those nickel particles cannot react with oxycarbonate species ($La_2O_2CO_3$). Consequently an irreversible carbon deposition occurs. The reactions involved when unreduced La_2NiO_4 are presented in Fig. 10. In spite of the important carbon deposition, no deactivation was observed within 20 h of reaction. This can be attributed to the fact that catalytic reaction is occurring at the Ni–$La_2O_2CO_3$ interfacial area which is not significantly affected by the carbon deposition during the time of reaction.

3.11. Characterization of carbon deposition

3.11.1. Thermogravimetric analysis

TGA analysis under air was performed using reduced and non-reduced La_2NiO_4 as starting material. This technique allows the quantification of the amount of carbon deposited on the surface of the catalyst during the CO_2/CH_4 reforming reaction. Fig. 11 shows the TGA profiles. The TGA data confirms that there was no carbon deposition when using the La_2NiO_4 perovskite used as precursor (Fig. 11a), whereas coke production occurs when La_2NiO_4 is used without treatment prior of reaction (Fig. 11b). Fig. 11a shows a weight loss of 3%, which corresponds to the carbon percentage in $La_2O_2CO_3$. Fig. 11b shows a weight loss of 70%, corresponding to the percentage of carbon deposited on the catalyst surface during reaction when using the non-reduced La_2NiO_4 as starting material.

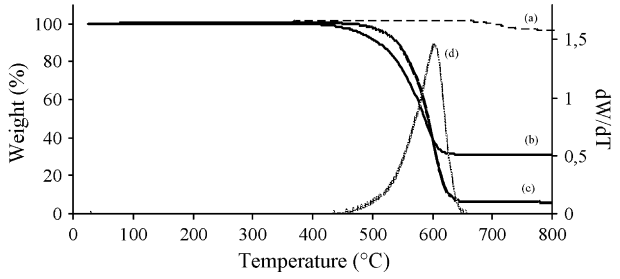

Fig. 11. TGA of the catalyst after reaction using: (a) reduced La_2NiO_4, (b) non-reduced La_2NiO_4, (c) non-reduced La_2NiO_4 after acid treatment and (d) differentiated TG curves of (c).

Acid treatment was used to dissolve the catalyst. The carbonaceous material was immersed in 65% HNO_3 for 1 h under continuous stirring. The product was filtered and washed with deionized water. The residue was then dried at 100 °C for 24 h.

Fig. 11c and d shows the TGA graph and the differentiated TGA of the acid-treated catalyst. The derivative of the weight loss profile presents a peak near 600 °C which suggests that there may be only one phase in the sample. Fig. 11c shows a weight loss of 94%, the remaining weight of 6% corresponding to nickel oxide particles.

3.11.2. TEM characterization

Fig. 12 shows TEM micrographs of the catalyst after the methane reforming reaction using the non-reduced La_2NiO_4. These micrographs provided clear evidence of the formation of multiwalled carbon nanotubes (MWCNT) during the reaction. The MWCNTs have a diameter distribution between 8–16 nm (inner diameter) and 20–40 nm (outer diameter). In general, the observed inner diameter of the MWCNT is almost equal to that of the Ni particle which forms the carbon nanotubes.

3.11.3. Raman characterization

Raman spectroscopy was employed to investigate the nature of carbon deposited on the surface of the catalyst during CO_2 reforming of CH_4 using non-reduced La_2NiO_4 as starting material. Fig. 13 shows the Raman spectrum obtained after acid treatment. The spectrum shows a strong peak at 1290 cm^{-1} (D band) and a peak at 1602 cm^{-1} (G band). These peaks positions are close to the 1346 and 1578 cm^{-1} which have been previously reported in the literature [56]. The peak at 1602 cm^{-1} (G band) corresponds to an E_{2g} vibration mode of graphite and is related to sp^2-bonded carbon atoms in a two-dimensional hexagonal lattice, such as in a graphite layer [57]. Carbon nanotubes with concentric multiwalled layers of hexagonal carbon lattice display the same vibration [58]. The peak near 1290 cm^{-1}, the so-called D band, indicates disordered sp^2-hybridized carbon atoms.

It is known that the relative intensity ratio of I_D/I_G can express the graphitization of carbon nanotubes or degree of disorder in the structure, which is the quality of the carbon nanotubes. Tan et al. [59] reported values of $I_D/I_G = 0.051$ for highly oriented pyrolytic graphite (highly organized), $I_D/I_G = 0.430$ for carbon nanotubes prepared by dc arc discharge

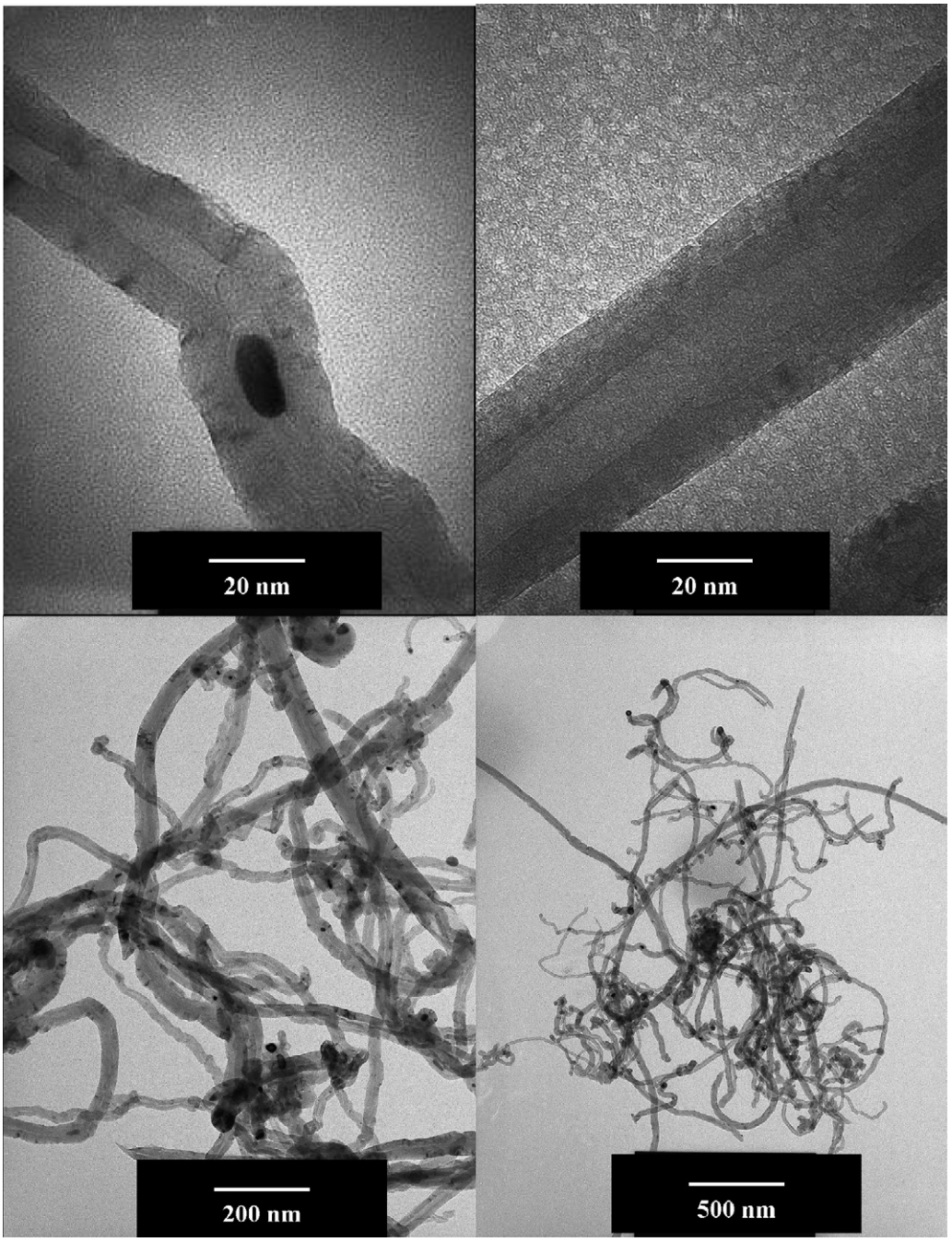

Fig. 12. TEM image of multiwalled carbon nanotubes (MWCNTs).

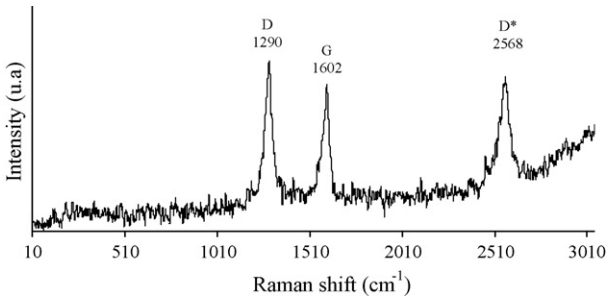

Fig. 13. Raman spectrum of carbon deposed during CO_2 reforming of CH_4 using non-reduced La_2NiO_4 as start material (treated with 65% HNO_3).

and $I_D/I_G = 3.56$ for CNT prepared by catalytic methods. In our case $I_D/I_G = 1.15$, indicates that the carbon nanotubes are very well graphitized, as confirmed by TGA. In the TGA profile (Fig. 11), the weight loss between 500 and 650 °C corresponds to the oxidation of carbon nanotubes, which is lower than the one reported by Ajayan et al. (700 °C) [60], but higher than that reported by Kukovitskii and Chernozatonskii (420 °C) [61].

Even though the nature of multiwalled layers was confirmed by TEM microscopy, the peak near 2568 (2D or D* peak) cm^{-1} suggests the formation of single wall nanotubes (SWCNT) during the methane dry reforming reaction.

4. Conclusions

We have shown that the reduction of the perovskite La_2NiO_4 leads to the formation of small nickel particles with an average diameter of 7 nm which would be responsible for the high activity.

The use of the reduced perovskite La_2NiO_4 as catalyst precursor shows the highest activity for the carbon dioxide reforming of methane, with CH_4 and CO_2 conversion of 85 and 93%, respectively, without carbon deposition after 160 h of reaction.

The molar ratio H_2/CO obtained is lower than 1 (equal to 0.93). This result was explained by the occurrence of the RWGS reaction.

During the reaction the CO_2 is adsorbed on La_2O_3 to form oxycarbonate species such as $La_2O_2CO_3$. The presence of these carbonate species would stabilize electronically the nickel particle hindering the sintering.

The absence of coke formation using the reduced La_2NiO_4 as catalyst precursor could be explained by the easy reaction between the $La_2O_2CO_3$ and the Ni–CH_x species to produce CO and H_2.

The use of the La_2NiO_4 without reductive treatment prior to the reaction leads to an important carbon deposition resulting mainly from methane decomposition. TEM and Raman analysis showed that multiwalled carbon nanotubes are formed in those experimental conditions.

Acknowledgements

The authors are grateful to COLCIENCIAS and CNRS for the support given to the PICS program: ''Valorization of natural gas and Fischer–Tropsch synthesis''.

F. Mondragón and G. Sierra acknowledge the financial support of the project Sostenibilidad by the University of Antioquia and the project no. 1115-06-17639 by COLCIENCIAS and the University of Antioquia. G. Sierra acknowledges COLCIENCIAS and the University of Antioquia for the PhD scholarship.

References

[1] I. Wender, Fuel Process. Technol. 48 (1996) 189.
[2] D.L. Trimm, Catal. Rev. Sci. Eng. 16 (1977) 155.
[3] S. Wang, G.Q. Lu, Energy Fuels 10 (1996) 896.
[4] M.F. Mark, F. Mark, W.F. Maier, Chem. Eng. Tech. 20 (1997) 361.
[5] E. Ruckenstein, H.Y. Wang, J. Catal. 205 (2002) 289.
[6] J.Z. Luo, Z.L. Yu, C.T. Au, J. Catal. 194 (2000) 198.
[7] S. Teuner, Hydrocarbon Process. 64 (1985) 106.
[8] S. Liu, G. Xiong, H. Dong, W. Yang, Appl. Catal. A: Gen. 202 (2000) 141.
[9] V.R. Choudhary, B.S. Uphade, A.S. Mamman, Appl. Catal. A: Gen. 168 (1998) 33.
[10] V.R. Choudary, A.M. Rajput, B. Prabhakar, Catal. Lett. 32 (1995) 391.
[11] A.M. Conner, J.R.H. Ross, Catal. Today 46 (1998) 203.
[12] R. Horn, K.A. Williams, N.J. Degenstein, L.D. Schmidt, Chem. Eng. Sci. 62 (2007) 1298.
[13] J. Nakamura, K. Akkawa, K. Sato, T.J.U. Chijima, Jpn. Petrol. Inst. 97 (1993) 36.
[14] J.S.H.Q. Perera, J.W. Couves, G. Sankar, J.M. Thomas, Catal. Lett. 11 (1991) 219.
[15] P.D.F. Vernon, M.L.H. Green, A.K. Cheetham, A.T. Ashcroft, Catal. Today 13 (1992) 417.
[16] A. ErdYohelyi, J. Cserenyi, F. Solymosi, Appl. Catal. A 108 (1994) 205.
[17] T. Inui, Catal. Today 51 (1999) 361.
[18] A.M. Efstathiou, A. Kladi, V.A. Tsipouriari, X.E. Verykios, J. Catal. 158 (1996) 64.
[19] Z.L. Zhang, V.A. Tsipouriari, A.M. Efstathiou, X.E. Verykios, J. Catal. 158 (1996) 51.
[20] J.R. Rostrup-Nielsen, J.H. Back Hansen, J. Catal. 144 (1993) 38.
[21] V.A. Tsipouriari, A.M. Efstathiou, Z.L. Zhang, X.E. Verykios, Catal. Today 21 (1994) 579.
[22] A. ErdYohelyi, J. Cserenyi, F. Solymosi, J. Catal. 141 (1993) 287.
[23] J. Rynkowski, P. Samulkiewicz, A.K. Ladavos, P.J. Pomonis, Appl. Catal. A: Gen. 263 (2004) 1.
[24] J. Wang, Y.-S. Wu, T.-J. Huang, Appl. Catal. A: Gen. 272 (2004) 289.
[25] S. Tomiyama, R. Takahashi, S. Sato, T. Sodesawa, S. Yoshida, Appl. Catal. A: Gen. 241 (2003) 349.
[26] J.R. Rostrup-Nielsen, Stud. Surf. Sci. Catal. 36 (1988) 73.
[27] Z. Zhang, X.E. Verykios, Appl. Catal. A: Gen. 138 (1996) 109–133.
[28] C. Batiot-Dupeyrat, G. Valderrama, A. Meneses, F. Martinez, J. Barrault, J.M. Tatibouët, Appl. Catal. A: Gen. 248 (2003) 143.
[29] C. Batiot-Dupeyrat, G.A. Sierra, F. Mondragón, J. Barrault, J.M. Tatibouët, Catal. Today 107–108 (2005) 474.
[30] P. Neumann, St.C. Teuner, F. Von Linde, Oil Gas Eur. Mag. 27 (2001) 44.
[31] G. Kurz, S. Teuner, Erdoel Erdgas Kohle, 43 (1990) 171.
[32] N.R. Udengaard, J.H. Bak Hansen, D.C. Hanson, J.A. Stal, Oil Gas J. 90 (1992) 62.
[33] H.C. Dibbern, P. Olesen, J.R. Rostrup-Nielsen, P.B. Tottrup, N.R. Udengaard, Hydrocarbon Process. 65 (1986) 71.
[34] J.R. Rostrup-Nielsen, J. Catal. 85 (1984) 31.
[35] J.R. Rostrup-Nielsen, Stud. Surf. Sci. Catal. 68 (1991) 85.
[36] F. Yagi, R. Kanai, S. Wakamatsu, R. Kajiyama, Y. Suehiro, M. Shimura, Catal. Today 104 (2005) 2.
[37] Z. Zhang, X.E. Verykios, J. Chem. Soc., Chem. Commun. (1995) 71.
[38] R. Pechini, US Patent No. 3,330,697 (1967).
[39] M.L. Fontaine, C. Laberty-Robert, F. Ansart, P. Tailhades, J. Solid State Chem. 177 (2004) 1471.
[40] R.F. Hicks, Q.J. Yen, A.T. Bell, J. Catal. 89 (1984) 498.
[41] T.H. Fleisch, R.F. Hicks, A.T. Bell, J. Catal. 87 (1984) 398.
[42] Z. Zhang, X.E. Verykios, S.M. MacDonald, S. Affrossman, J. Phys. Chem. 100 (1996) 744.
[43] W.S. Dong, H.S. Roh, K.W. Jun, S.E. Park, Y.S. Oh, Appl. Catal. A: Gen. 226 (2002) 63.
[44] X.E. Verykios, Int. J. Hydrogen Energy 28 (2003) 1045.
[45] Z. Hao, H.Y. Zhu, G.Q. Lu, Appl. Catal. A 242 (2003) 275.
[46] G. Sierra Gallego, F. Mondragón, J. Barrault, J.M. Tatibouët, C. Batiot-Dupeyrat, Appl. Catal. A: Gen. 311 (2006) 164.
[47] B.S. Liu, L.Z. Gao, C.T. Au, Appl. Catal. A: Gen. 235 (2002) 193.
[48] J.Z. Luo, L.Z. Gao, Z.L. Yu, C.T. Au, Stud. Surf. Sci. Catal. 130 (2000) 689.
[49] J. Guo, H. Lou, Y. Zhu, X. Zheng, Mater. Lett. 57 (2003) 4450.
[50] Z. Zhang, X.E. Verykios, Appl. Catal. A: Gen. 138 (1996) 109.
[51] V.A. Tsipourai, X.E. Verykios, Catal. Today 64 (2001) 83.
[52] V.A. Tsipouriari, X.E. Verykios, J. Catal. 187 (1999) 85.
[53] Z. Kalenik, E.E. Wolf, Catal. Lett. 11 (1991) 309.
[54] H.Q. Yang, Y.Q. Chen, C.H. Hu, M.C. Gong, H.R. Hu, A.M. Tian, N.B. Wong, Chem. Phys. Lett. 355 (2002) 233.
[55] R.A. Cambell, J. Szanyi, P. Lenz, D.W. Goodman, Catal. Lett. 17 (1993) 39.
[56] H.-B. Zhang, G.-D. Lin, Z.-H. Zhou, X. Dong, T. Chen, Carbon 40 (2002) 2429.
[57] F. Tuinstra, J.L. Koening, J. Chem. Phys. 53 (3) (1970) 1126.
[58] A.G. Souza Filho, A. Jorio, G.G. Samsonidze, G. Dresselhaus, R. Saito, M.S. Dresselhaus, Nanotechnology 14 (2003) 1130.
[59] P. Tan, S. Zhang, K. To Yue, F. Huang, J. Raman Spectrosc. 28 (1997) 369.
[60] P.M. Ajayan, T.W. Ebbesen, S. Iijama, Nature 362 (1993) 522.
[61] E.F. Kukovitskii, L.A. Chernoszatonskii, Chem. Phys. Lett. 266 (1997) 323.